Clays and Clay Minerals, Vol. 45, No. 5, 690–708, 1997.

COMPARISON OF HEMATITE COAGULATION BY CHARGE SCREENING AND PHOSPHATE ADSORPTION: DIFFERENCES IN AGGREGATE STRUCTURE

JON CHOROVER,[1,2] JINGWU ZHANG,[1] MARY KAY AMISTADI[2] AND JACQUES BUFFLE[1]

[1] Department of Inorganic, Analytical and Applied Chemistry, University of Geneva, Sciences II, 1211 Geneva 4, Switzerland

[2] Department of Agronomy, The Pennsylvania State University, University Park, Pennsylvania 16802-3504

Abstract—The formation and structure of hematite aggregates were examined by dynamic and static light scattering techniques. A large range in coagulation kinetics was studied by varying either indifferent electrolyte (KCl) concentration or surface complexing anion ($H_2PO_4^-$) concentration, P_T, at pH 6.0 ± 0.1. Diffusion limited aggregation (DLA) was induced by counterion screening at [KCl] > 80 mM or by surface charge neutralization at P_T = 31 μM (and ionic strength = 1.0 mM). In DLA, the fractal dimension, d_f, of aggregates formed by either surface charge neutralization or counterion screening was 1.7 ± 0.1. A reduction in the rate of coagulation in KCl for [KCl] < critical coagulation concentration (CCC) produced an increase in d_f to 2.1 ± 0.1. For aggregation induced by phosphate adsorption at constant ionic strength, there was no apparent trend in d_f with coagulation rate. The value of d_f was consistently less than 1.8 when reaction limited aggregation (RLA) resulted from surface charge neutralization rather than counterion screening. TEM observations of aggregates formed in the presence or absence of phosphate confirm that, when RLA is induced by phosphate adsorption, resulting aggregates are much looser in structure than those formed by counterion screening. The results suggest that the high-affinity binding of phosphate to hematite may result in a nonrandom distribution of surface charge that facilitates the coalescence of positive and negative charge crystal faces.

Key Words—Coagulation Kinetics, Fractal Aggregate, Hematite, Light Scattering, Phosphate Adsorption.

INTRODUCTION

Aqueous-phase chemistry affects the stability of colloidal suspensions by influencing the magnitude and range of particle surface charge. In the presence of indifferent electrolyte, coagulation rate is a function of electrolyte concentration, and rapid coagulation is induced by a reduction in the range of the electrostatic repulsive force as counterion concentration in the vicinity of particle surfaces is increased. In other words, counterion screening induces coagulation (Hunter 1987). At constant ionic strength, the coagulation rate may be altered by changing the concentration of ions that form inner-sphere complexes with the mineral surface, thereby directly affecting the magnitude of surface charge. In the latter case, coagulation is induced by surface charge neutralization and rapid coagulation occurs around the aqueous concentration of specifically adsorbing electrolyte that produces a net zero charged surface, that is, at the point of zero charge, p.z.c. (O'Melia 1989; Sposito 1992). The structure of aggregates is often a function of coagulation rate and, in some cases, can be predicted from the time evolution of aggregate size (Meakin 1991).

Colloidal aggregates can be characterized quantitatively by employing concepts of fractal geometry (Jullien and Botet 1987; Pfeifer and Obert 1989; Lin et al. 1989; Zhang and Buffle 1996). Fractals are objects that usually exhibit complex and irregular (non-Euclidean) structure that is self-similar over a range of length or time scales (Pfeifer and Obert 1989). The coagulation of primary particles into aggregates, followed by the combination of small aggregates into larger ones, termed "cluster–cluster aggregation" (Jullien and Botet 1987), produces a fractal object, which can be characterized on the basis of its fractal dimension, d_f. In contrast to a compact aggregate, in which the number of primary particles, N, and the aggregate spatial extent, R, are related as $N \sim R^3$, the number of primary particles in a fractal object is related to its characteristic length by $N \sim R^{df}$, where $d_f < 3$ (Pfeifer and Obert 1989).

Cluster–cluster aggregation comprises 2 limiting kinetic regimes: DLA and RLA (Jullien and Botet 1987). In DLA, the rate-limiting step is the movement of 2 particles toward each other prior to encounter and formation of a larger particle. Although the equilibrium state of an aggregate should be compact, when an aggregate is locked into a configuration set by initial contact, a much less dense system is formed (Evans and Wennerström 1994). During DLA, aggregates of particles collide and combine instantaneously, without optimizing packing density into a close-fitting, organized structure. The resulting aggregate is porous and convoluted. The theoretical value of d_f for aggregates formed in the DLA regime is ≈ 1.8 (Jullien and Botet 1987) and experiments on colloidal gold, silica, polystyrene, latex and iron oxide are in agreement (Lin

Copyright © 1997, The Clay Minerals Society

Downloaded from https://www.cambridge.org/core. 16 Nov 2026 at 11:32:43, subject to the Cambridge Core terms of use.

et al. 1989; Zhang and Buffle 1996). Reaction limited aggregation occurs when there is a significant potential barrier so that the sticking probability upon particle–particle interaction is less than unity (Sposito 1994). Simulation modeling and numerous experimental investigations of RLA have produced aggregates with $d_f \approx 2.1$ (Weitz et al. 1985; Jullien and Botet 1987; Lin et al. 1989; Meakin 1991; Zhang and Buffle 1996), indicating that a more compact aggregate structure is formed under conditions of slow coagulation. Zhang and Buffle (1996) used light scattering and transmission electron microscopy (TEM) methods to measure d_f of hematite aggregates formed in KCl solutions at pH 3. They found that d_f decreases from approximately 2.2 to approximately 1.8 as [KCl] increases above 100 m*M* and the coagulation regime passes from RLA to DLA (Zhang and Buffle 1996).

The sorption of phosphate by Fe (hydr)oxide particles has been the subject of extensive research for the past 20 years because of its environmental and geochemical significance. The formation of surface complexes between orthophosphate and hydroxyl surface functional groups affects particle surface charge and colloidal behavior (Parfitt and Atkinson 1976; Parfitt et al. 1976; Sigg and Stumm 1981; Tejedor–Tejedor and Anderson 1990; Liang and Morgan 1990). Liang and Morgan (1990) found that the onset of rapid coagulation for hematite (α-Fe_2O_3) occurred at phosphate concentrations 100 times lower than those predicted for counterion screening according to Derjaguin–Landau–Verwey–Overbeek (DLVO) theory (Verwey and Overbeek 1948) and the discrepancy was attributed to particle charge reduction resulting from surface complexation. Relatively few systematic comparisons of coagulation induced by 1) counterion screening versus 2) surface complexation have been reported (Liang and Morgan 1990), and there is no study of the effect that specific adsorption reactions may have in governing the formation and structure of colloidal aggregates. Therefore, the objectives of the present study were to 1) measure the rate of hematite coagulation as a function of counterion screening and surface complexation and 2) examine the structural properties of the resulting aggregates at constant pH. A slightly acidic pH regime (pH 6) was chosen to model the pH of natural waters. At pH 6, orthophosphate exists predominantly as monovalent $H_2PO_4^-$, with small quantities (<5% of total orthophosphate) as bivalent HPO_4^{2-} (Stumm and Morgan 1996).

MATERIALS AND METHODS

Synthesis of Hematite Colloids

Hematite colloids were prepared using a modification of the method of Penners and Koopal (1986). All solutions were prepared from Milli-Q Plus® deionized water and were passed through 0.2-μm Millipore® filters, prerinsed with Milli-Q Plus water, to remove any contaminant particles. A concentrated stock solution of $FeCl_3$ was prepared from Merck reagent grade $FeCl_3 \cdot 6H_2O$ at 1.82 *M* to minimize hydrolysis of Fe^{3+} at room temperature. An aliquot of the stock solution was diluted with H_2O and HCl to produce a solution of 0.72 *M* $FeCl_3$ and $3.75 \cdot 10^{-3}$ *M* HCl, which was then filtered. A solution of 0.975 L of $3.75 \cdot 10^{-3}$ *M* HCl was heated to boiling in a 1-L borosilicate glass bottle. Twenty-five mL of the $FeCl_3$/HCl solution were quickly added to the boiling HCl under conditions of vigorous mixing with a magnetic stirrer. The bottle was capped and placed in an oven at 100 °C for 24 h. After the bottle was removed from the oven, the contents were left to cool at room temperature for several hours. The suspension was then transferred to prewashed Cellu-Step® regenerated cellulose membrane dialysis tubing with a molecular weight cutoff of 12,000–14,000 (roughly 3.0 nm nominal pore size) and dialyzed against 10^{-3} *M* HCl for 2 weeks. For the first several days of dialysis, the HCl solution was changed daily and after 3–4 d the solution was changed every 2 d. The solid concentration of the final suspension (after dialysis) was determined by adding a measured mass of suspension (approximately 12 g) to each of 5 ceramic weighing dishes and drying contents to constant mass. The remaining suspension was stored in a plastic bottle at 4 °C. Prior to experiments, an aliquot of stock hematite suspension was diluted to a total solid concentration of 100 mg kg^{-1} with 10^{-3} *M* HCl in a 60-mL high density polyethylene (HDPE) container. This suspension was used as the source of hematite for all experiments and was prepared again at intervals of less than 7 d. Synthetic hematite particles were nearly spherical, with an average radius of 26 ± 2 nm as determined by TEM analysis.

Electrophoretic Mobility of Hematite as a Function of P_T

Electrophoretic mobility of hematite primary particles and aggregates was measured by laser velocimetry (Malvern Zetasizer III® equipped with a 700-mW Ar laser, λ = 488 nm). Electrophoretic mobilities (u) are calculated from the ratio of steady-state particle velocity and the magnitude of the applied electrical field. All experimental solute concentrations are expressed in moles per kilogram of solution. Stock solutions of KCl, KH_2PO_4, KOH and Milli-Q H_2O were combined to produce a solution that, upon mixing with 20 mg kg^{-1} hematite suspended in $2 \cdot 10^{-4}$ mol kg^{-1} HCl, produced a suspension of 1.0 mmol kg^{-1} ionic strength (I) at pH 6.0 ± 0.1 and variable total phosphate concentrations (P_T) ranging from 10^{-6} to $10^{-3.06}$ mol kg^{-1}. Fifty grams of 20 mg kg^{-1} hematite suspension was prepared by diluting 10.0 g of 100 mg kg^{-1} stock with 40.0 g Milli-Q H_2O in a 50-mL HDPE container and 50.0 g of KCl/KH_2PO_4/KOH solution was

Downloaded from https://www.cambridge.org/core. 16 Nov 2026 at 11:32:43, subject to the Cambridge Core terms of use.

prepared from stock solutions in a 125-mL HDPE container. Preliminary titration experiments indicated the quantity of base required to reach pH 6.0 for different KH_2PO_4 concentrations. Final solid concentrations of experimental suspensions were 10 mg kg^{-1}. At 5, 85, 245 and 440 min after mixing of hematite with KCl/KH_2PO_4/KOH solutions, a new 10-mL aliquot of each experimental suspension was withdrawn and injected into the electrophoresis cell. The cell was cleaned prior to injection of each new aliquot to remove any hematite particles adsorbed to the cell walls. At least 4 successive measurements of u were made for each sample injection and the average was then calculated. All experiments were performed in duplicate and the duplicate mean is reported.

Phosphate Sorption Experiments

The sorption of orthophosphate to colloidal hematite was measured as a function of time and orthophosphate concentration (P_T) at pH 6.0 and I = 1.0 mmol kg^{-1} (KCl). Suspensions of 0.10 kg total mass were prepared with P_T ranging from 10^{-6} to $10^{-3.06}$ mol kg^{-1}, as detailed in the previous section. At time t = 0, hematite was combined with the KCl/KH_2PO_4/KOH solution and mixed by inverting 3 times. A 10-mL sample was extracted immediately by syringe and passed through prewashed Millipore cellulose nitrate 0.45-μm and 0.025-μm filters in series. The prewashing procedure consisted of passing 10 mL of Milli-Q H_2O through each filter. The first 3 mL of sample solution was discarded and then 5 mL was delivered to a polystyrene sample vial. Sampling was repeated 5, 15, 45, 85, 245 and 425 min, and 24 h after mixing. The vials were capped and stored at 4 °C prior to analysis. Storage never exceeded 48 h. Blank solutions were prepared, with P_T concentrations identical to the time t = 0 P_T values for the suspensions, and stored at 4 °C in polystyrene vials for the same duration. The measured orthophosphate concentrations of these "blanks" provided the time zero values for P_T. Dissolved orthophosphate concentrations in samples and blanks were measured colorimetrically by absorbance at 880 nm following molybdate blue reaction (Murphy and Riley 1962) in a Technicon II autoanalyzer. Dissolved Fe was measured by atomic absorption spectrometry. All standards and dilutions were prepared on a mass basis in the same KCl solution matrices used in the sorption experiments. The surface excess of orthophosphate was calculated on the basis of loss from solution:

$$\Gamma_P = \frac{P_0 - P_i}{C_{hem}} \quad [1]$$

where Γ_P is the quantity of orthophosphate sorbed to hematite (mol kg^{-1} hematite), P_0 and P_i are the dissolved concentrations orthophosphate at time t = 0 and time t = i, respectively (mol kg^{-1}), and C_{hem} is the concentration of hematite in the suspension (mg kg^{-1}). All adsorption measurements were performed in triplicate and mean values are reported.

Coagulation Kinetics and Aggregate Structure

The evolution of particle size as a function of solution chemistry and time was measured by photon correlation spectroscopy (PCS) using a Malvern 4700 PCS spectrometer equipped with a 700-mW Ar laser. The method involves laser illumination of a particle suspension, with measurement of the autocorrelation of the time-dependent scattered-photon intensity. The mean hydrodynamic diameter (d_z) of the particles or aggregates, which by definition is inversely proportional to their diffusion coefficient, is obtained from a cumulant analysis of the log-transformed autocorrelation function of scattered intensity by standard numerical fitting methods (Pecora 1985; Schurtenberger and Newman 1993; Zhang and Buffle 1995).

Experiments were performed at 25 ± 0.1 °C and a scattering angle of 45°. This moderately low angle scattering yields a slightly lower signal-to-noise ratio than higher scattering angles, but provides a more accurate measure of the translational diffusion coefficient because the contribution of rotational diffusion increases as a function of scattering vector (Pecora 1985). Hematite suspensions were prepared at pH 6.0 and *either* variable indifferent electrolyte concentration (KCl = 1–100 mmol kg^{-1}) *or* I = 1.0 mmol kg^{-1} with variable ratio of KH_2PO_4 to KCl, as in the electrophoretic mobility experiments. The time-dependent variation in mean d_z was measured by PCS. At time t = 0, 20 mg kg^{-1} hematite at pH 4 was mixed with an equal mass of KCl/KH_2PO_4/KOH solution, inverted 3 times and an aliquot of the experimental suspension was placed into the goniometer sizing cell. The d_z was measured as a function of time and individual determinations were made over 10-s durations for the initial stages of DLA, with an average incremental increase in measured d_z of less than 5% between measures.

Aggregate structures were determined by TEM and static light scattering (SLS). For selected aggregation experiments, a sample aliquot was taken from the large suspension vessel after d_z reached approximately 1.0 μm. A 50-μL sample was gently mixed with 5 μL of Nanoplast FB101, a melamime resin that has hydrophilic properties (Frosch and Westphal 1989), on a Teflon plate. A carbon-coated TEM grid was immersed in the solution, then centrifuged vertically at 7000 relative centrifugal force for 30 s and stored after drying, prior to examination with a Jeol 1200 EX-II TEM (Perret et al. 1992).

Static light scattering was used to determine the fractal dimension of colloidal aggregates, following the kinetic experiments, when the aggregates comprised a large number of primary particles and d_z was on the order of 1.0 μm. The use of SLS to determine d_f has been dis-

Downloaded from https://www.cambridge.org/core. 16 Nov 2026 at 11:32:43, subject to the Cambridge Core terms of use.

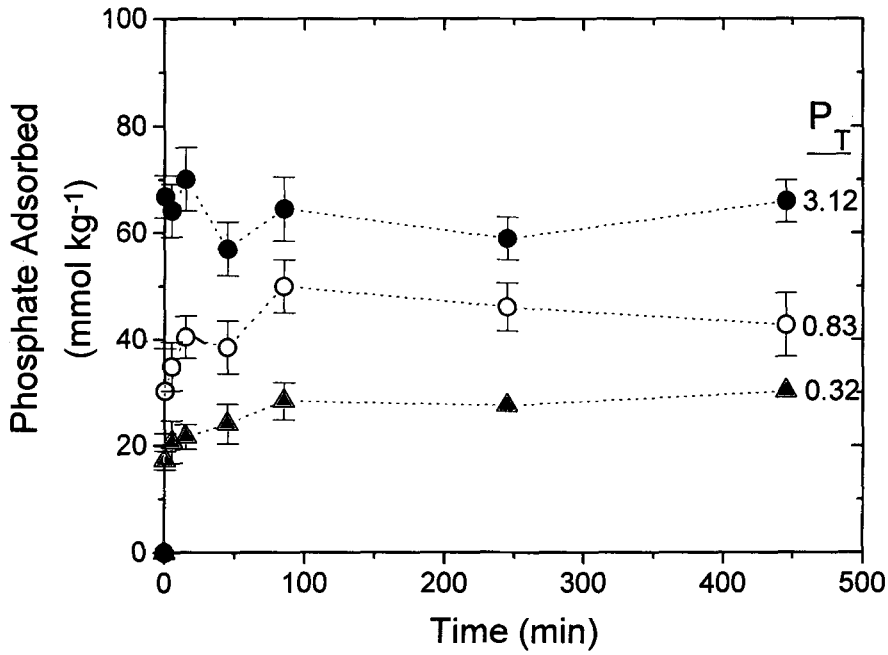


Figure 1. Surface excess of phosphate versus time. Total suspension phosphate concentration, P_T, (μmol kg^{-1}) is indicated on right side of graph. Error bars indicate standard deviation of triplicate samples. Hematite concentration = 10 mg L^{-1}, pH = 6.0, I = 1.0 mM, T = 25 °C.

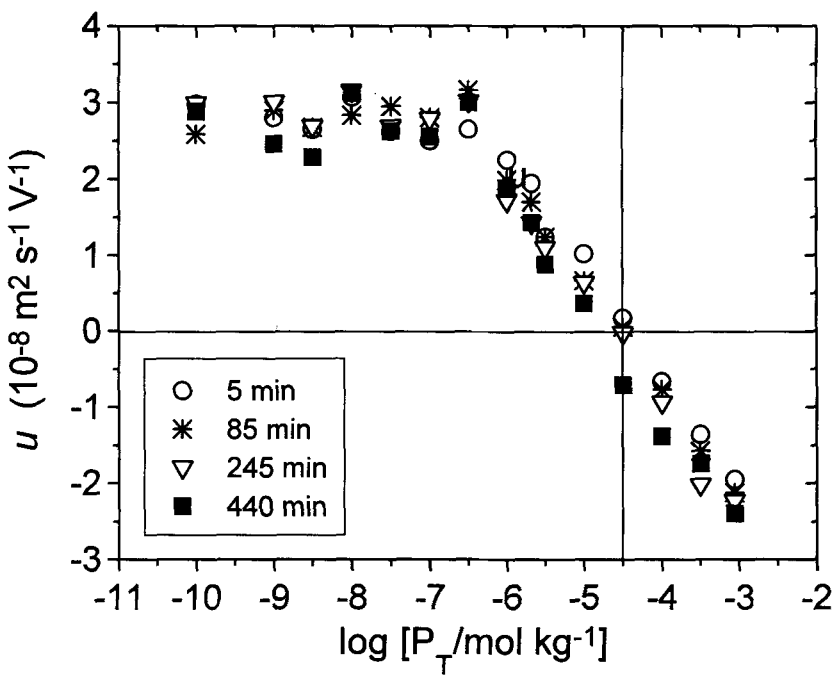


Figure 2. Electrophoretic mobility (u) of hematite as a function of total phosphate concentration and reaction time. Hematite concentration = 10 mg L^{-1}, pH = 6.0, I = 1.0 mM, T = 25 °C.

Downloaded from https://www.cambridge.org/core. 16 Nov 2026 at 11:32:43, subject to the Cambridge Core terms of use.

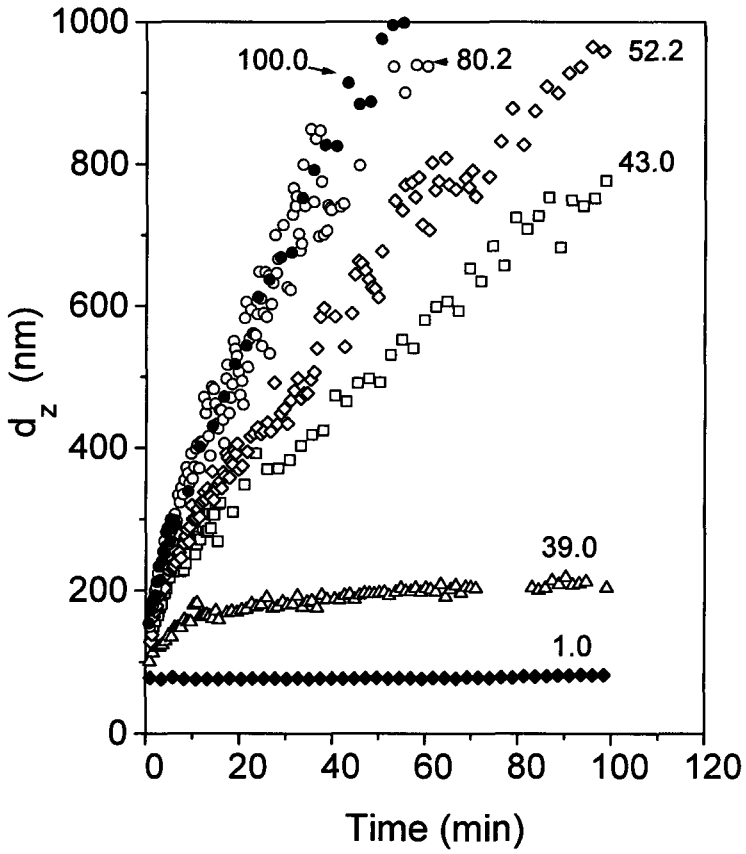


Figure 3. Size evolution of hematite aggregates, as measured by PCS, at KCl concentrations indicated adjacent to curves. Concentration units are mmol kg^{-1}. Diffusion limited aggregation is observed at 80 mmol kg^{-1} KCl. Hematite concentration = 10 mg L^{-1}, pH = 6.0, T = 25 °C.

cussed elsewhere (Teixeira 1986; Lin et al. 1989; Schmidt 1989; Zhang and Buffle 1996). The time-averaged intensity of scattered light was measured as a function of wavevector, q (nm^{-1}), for θ ranging from 20 to 150°, where $q = (4\pi n/\lambda)\cdot\sin(\theta/2)$, n is the refractive index of the suspending solution, θ is the scattering angle and λ (nm) is the wavelength of incident radiation (488 nm). A minimum of 5 photon counts of 5 s each were made at each q and then averaged.

Data Analysis

The fractal dimensions of hematite aggregates were calculated using dynamic scaling and SLS techniques. The dynamic scaling method is limited to the DLA regime where it is assumed that aggregates grow via cluster–cluster aggregation and coagulation is irreversible. The average number of primary particles in an aggregate, m, increases linearly with time, t (Zhang and Buffle 1995):

$$m = 1 + k_s C_0 t \quad [2]$$

where k_s is the Smoluchowski rate constant and C_0 is the initial concentration of primary particles. The collision rate constant, k_s, is assumed to be independent of aggregate size and equivalent to that for two primary particles. The number of primary particles in a fractal aggregate is a power law function of its radius of gyration, R_g:

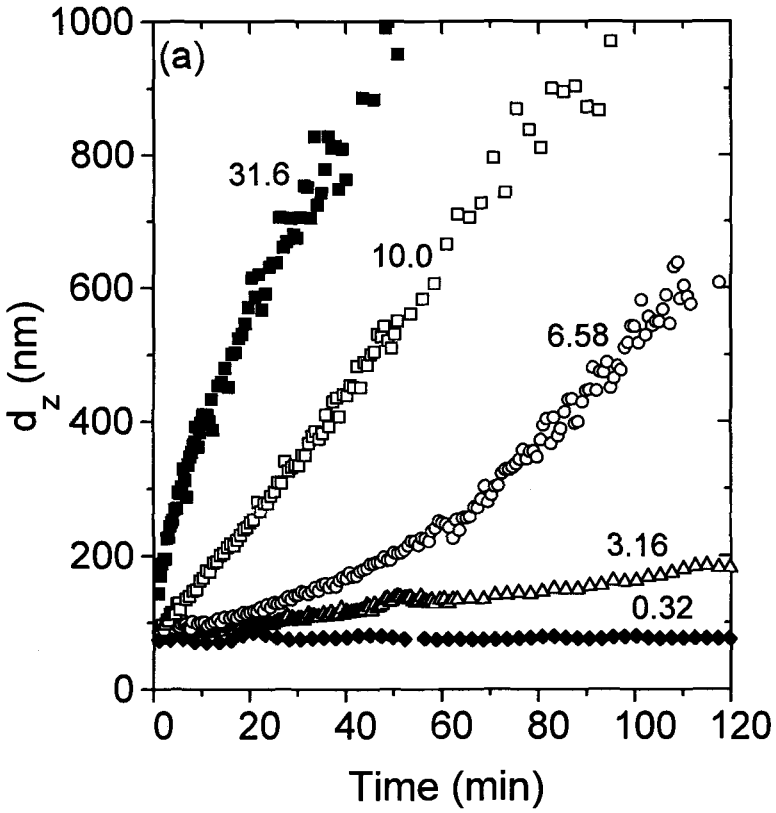
$$m \propto \left(\frac{R_g}{r_0}\right)^{d_f} \quad [3]$$

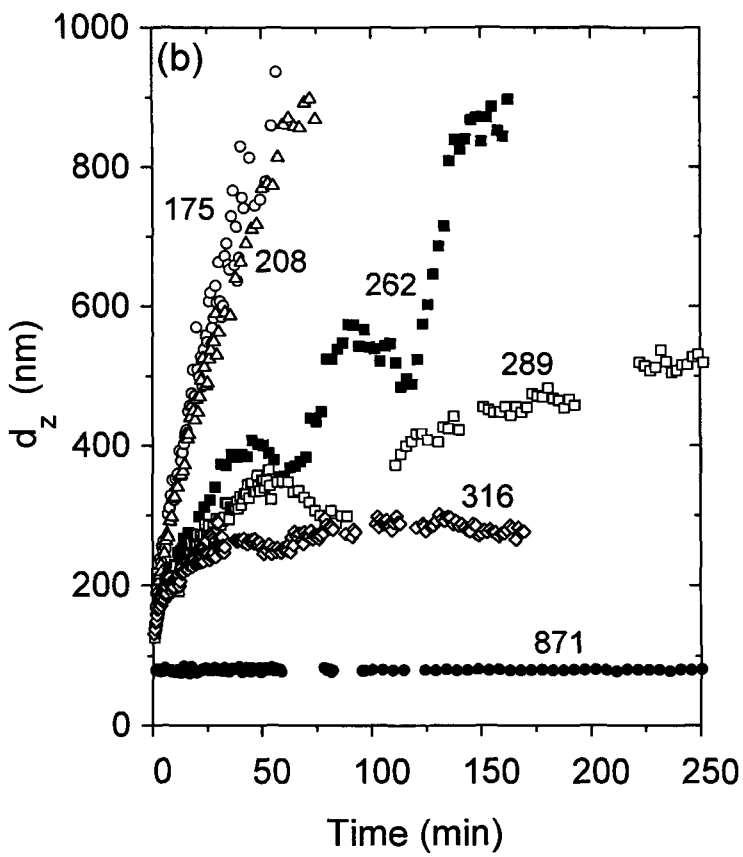
where r_0 is the radius of a primary particle. Substitution of Equation [2] into Equation [3] gives:

→

Figure 4. Size evolution of hematite aggregates for particles that are (a) net positive charged and (b) net negative charged. Total phosphate concentrations (in μmol kg^{-1}) are indicated adjacent to curves. Diffusion limited aggregation is observed in the region of the p.z.c. (P_T = 32 μmol kg^{-1}). Hematite concentration = 10 mg L^{-1}, pH = 6.0, I = 1.0 mM, T = 25 °C.

Downloaded from https://www.cambridge.org/core. 16 Nov 2026 at 11:32:43, subject to the Cambridge Core terms of use.





Downloaded from https://www.cambridge.org/core. 16 Nov 2026 at 11:32:43, subject to the Cambridge Core terms of use.

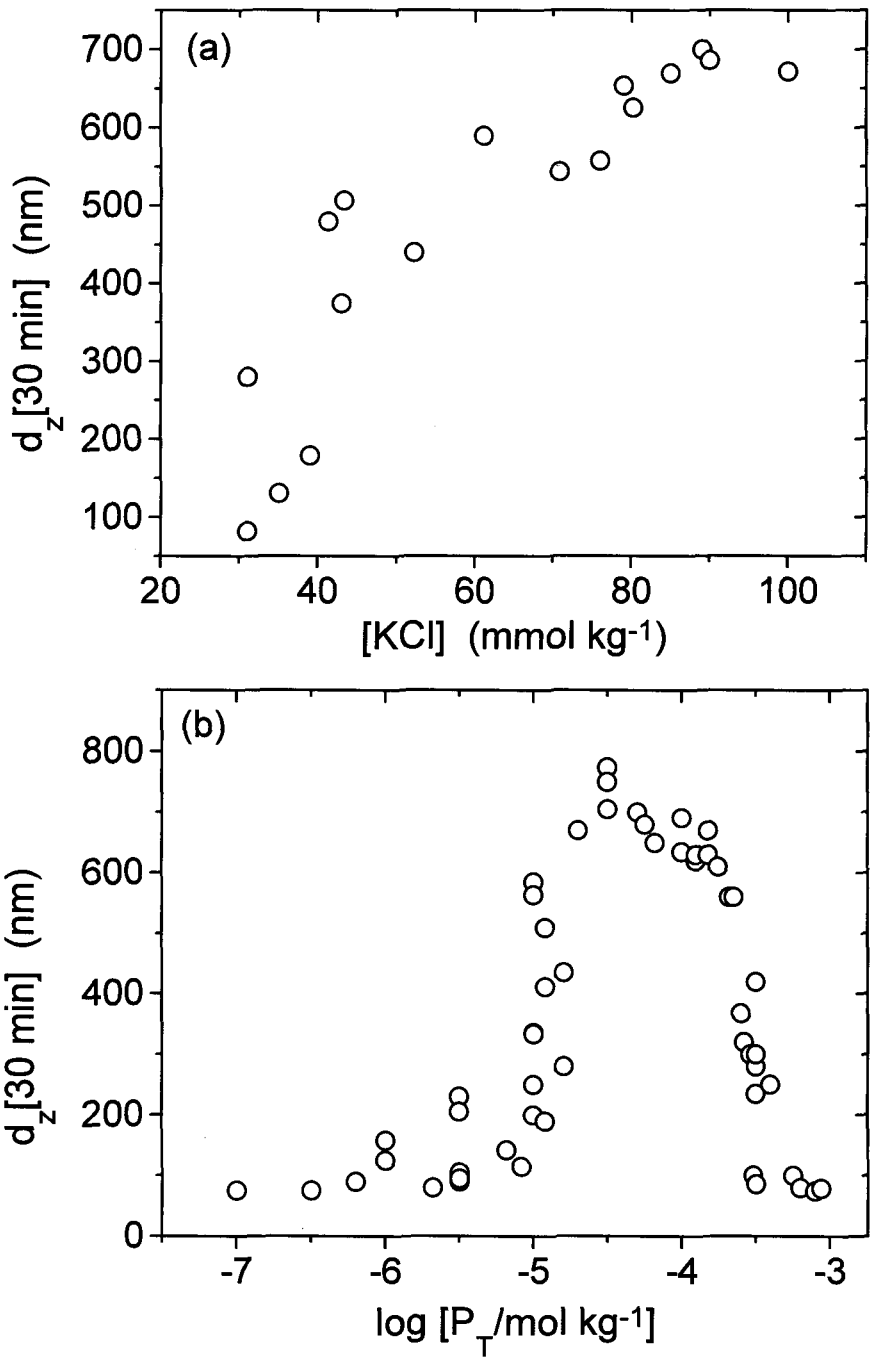


Figure 5. Summary of kinetic data. Hydrodynamic diameter of hematite particles after 30 min coagulation time as a function of (a) KCl and (b) phosphate concentrations. Coagulation rate at short time (<2.5 min) is shown in terms of relative stability, S_R, as a function of (c) KCl and (d) phosphate concentration. Error bars indicate 95% confidence interval. Hematite concentration = 10 mg L^{-1}, pH = 6.0, T = 25 °C.

$$R_g = r_0(1 + k_s C_0 t)^{1/d_f} \approx r_0(k_s C_0 t)^{1/d_f} \quad [4]$$

The approximation is valid when $k_s C_0 t \gg 1$. Zhang and Buffle (1995) showed that R_g is directly proportional to the hydrodynamic diameter, d_z, as measured by PCS under the present experimental conditions. Therefore, for DLA, a plot of log d_z versus log t should be a straight line with a slope of $1/d_f$.

The value of d_f in both RLA and DLA regimes may be determined using the static light scattering data. For $qr_0 \ll 1$ and $q\xi \gg 1$, where ξ is the characteristic

Downloaded from https://www.cambridge.org/core. 16 Nov 2026 at 11:32:43, subject to the Cambridge Core terms of use.

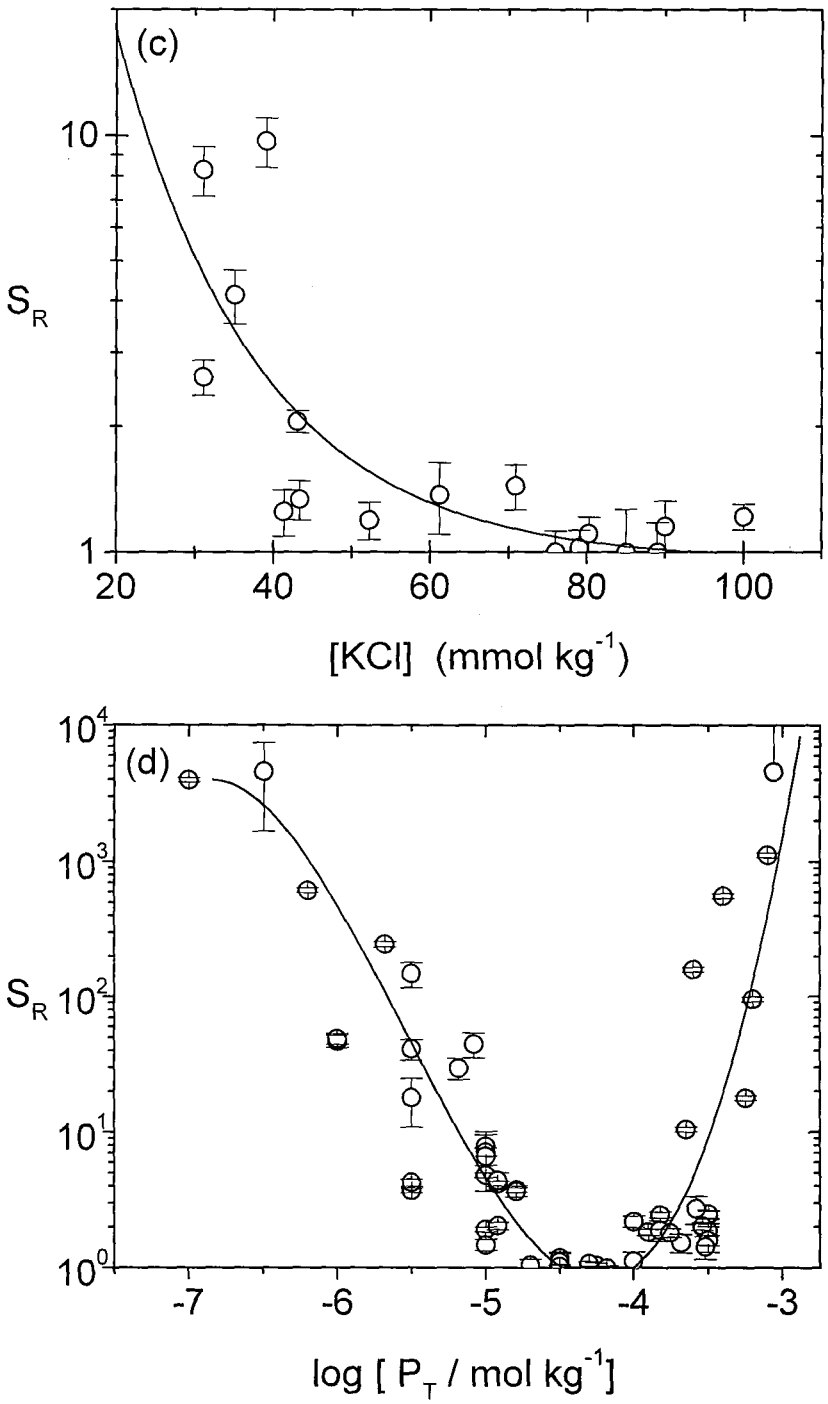


Figure 5. Continued

distance above which aggregate mass distribution no longer follows the fractal law, the scattered intensity, I, is a power law function of q (Teixera 1986):

$$I(q) \propto q^{-d_f} \quad [5]$$

and a plot of log I versus log q yields a straight line with slope $-d_f$. The value of ξ is accessible if a cutoff function is defined to account for the influence of finite aggregate size on the light scattering behavior (Schmidt 1989; Zhang and Buffle 1996). Since the precise nature of this function is not known, an exponential form is often used, in which case the value of ξ is

Downloaded from https://www.cambridge.org/core. 16 Nov 2026 at 11:32:43, subject to the Cambridge Core terms of use.

related to the radius of gyration, R_g, of the aggregate by (Teixeira 1988):

$$\xi = R_g\sqrt{\frac{2}{d_f(d_f + 1)}} \quad [6]$$

RESULTS

Phosphate Adsorption

As a result of chemical interactions, the magnitude of phosphate adsorbed to iron oxides is sensitive to the surface site/dissolved phosphate concentration ratio (Anderson et al. 1985). Therefore, to maintain consistent particle surface chemistry, the same particle concentration was used in adsorption, electrophoresis and coagulation experiments (10 mg kg^{-1}). At $P_T >$ 10 μmol kg^{-1}, it is difficult to quantify precisely the small difference between 2 relatively large quantities (numerator of Equation [1]) and so reliable adsorption data are limited to lower values of P_T. Adsorption kinetic data are presented in Figure 1 for P_T = 0.32, 0.83 and 3.12 μmol kg^{-1}. The quantities of P adsorbed are comparable to values reported by others for iron oxides suspended in similar aqueous media (Sigg and Stumm 1981; Anderson et al. 1985). Most of the phosphate adsorbed within the time frame of the experiment (24 h) is removed from solution within the first few minutes of reaction. The initial uptake may be followed by a subsequent desorption and readsorption, etc., as suggested for the higher concentrations of P_T in Figure 1. Oscillations in mean uptake were observed in numerous experiments, although those depicted in Figure 1 are within the 95% confidence interval for each time series. Oscillatory kinetic data have been reported for phosphate adsorption to goethite (Anderson et al. 1985) and the authors suggested that the oscillations result from coagulation processes, which produce the expulsion of phosphate to solution, over the course of the experiment.

Surface Charge

The effect of total phosphate concentration, P_T, on hematite surface charge is presented in Figure 2. At pH 6.0 and $P_T \leq 10^{-6.5}$ mol kg^{-1}, electrophoretic mobility (u) values are relatively constant, in the range of 2.7×10^{-8} m^2 s^{-1} V^{-1}. These values are slightly lower than 3×10^{-8} m^2 s^{-1} V^{-1} measured concurrently for the same hematite particles suspended in 1.0 mmol kg^{-1} HCl (pH 3). However, at $P_T > 10^{-6.5}$, a linear decrease in u is observed. The isoelectric point (i.e.p.) or p.z.c. is $P_T = 10^{-4.5}$ and charge reversal occurs with further increase in P_T (> 32 μmol kg^{-1}). A high, negative value of $u = -2.5 \times 10^{-8}$ m^2 s^{-1} V^{-1} was observed at maximum experimental phosphate concentration (0.87 mmol kg^{-1}). Above log $P_T = -6.5$, a slight decrease in u was observed with increased equilibration time, which is consistent with increased phosphate adsorption over the course of the experiment, as shown in Figure 1. The same temporal trend was observed for negatively charged particles ($P_T > 10^{-5}$). In this case, the magnitude of particle electrophoretic mobility increases with time and, therefore, the decrease in u cannot be attributed to particle size effects associated with coagulation processes.

Coagulation Kinetics

In the absence of phosphate, hematite suspensions are kinetically stable at pH 6.0 and 1.0 mmol kg^{-1} KCl; the d_z observed is equal to the d_z of primary particles (Figure 3). Reaction limited aggregation is observed for [KCl] > 10 mmol kg^{-1}. The rapid increase in hydrodynamic size observed immediately following mixing at [KCl] < 40 mmol kg^{-1} may result from accelerated aggregation during the mixing process. A large increase in coagulation rate is observed as KCl concentration is increased from 39 to 43 mmol kg^{-1} (Figure 3). However, coagulation rate increases to the diffusion limiting case only as [KCl] approaches 80 mmol kg^{-1} (Figure 3). No increase in coagulation kinetics was observed between 80 and 200 mmol kg^{-1} KCl. Therefore, 80 mmol kg^{-1} KCl represents the critical coagulation concentration (Sposito 1994); hematite coagulation is transport limited in 80 mmol kg^{-1} KCl solution at pH 6.

At a total ionic strength of 1.0 mmol kg^{-1}, suspension instability is induced at very low phosphate concentrations (Figure 4a). Slow coagulation is observed within 2 h as P_T is increased to 1.0 μmol kg^{-1}, corresponding to the onset of the decrease in particle surface charge (Figure 2), with $u \approx 2 \times 10^{-8}$ m^2 s^{-1} V^{-1}. Coagulation rate increases to the diffusion limiting case with increasing phosphate concentration toward the p.z.c. There is no further increase in coagulation rate above P_T = 32 μmol kg^{-1}, but a progressive decrease is observed at P_T > 100 μmol kg^{-1} (Figure 4b). Oscillations in size vs. time data were observed at high P_T (Figure 4b), possibly reflecting fragmentation and reorganization processes (see Discussion section). The decrease in coagulation rate at high P_T is consistent with the linear increase in $|u|$ (Figure 2) and associated repulsive interparticle forces (Hunter 1987). The suspension prepared at 871 μmol kg^{-1} P_T (Figure 4b) was stable for more than 3 d.

The value of d_z at 30 min is plotted versus KCl concentration in Figure 5a and P_T concentration in Figure 5b. At short reaction times where $t < 2.5$ min, the time evolution of d_z has been found to be linear with $r^2 > 0.95$ for $p < 0.001$. Therefore, the relative stability (S_R), defined as the rate of diffusion limited coagulation, R_{DLA}, divided by the rate of coagulation measured in a given experiment, R_{exp}, can be determined from linear regression of d_z against t, for $t <$ 2.5 min:

Downloaded from https://www.cambridge.org/core. 16 Nov 2026 at 11:32:43, subject to the Cambridge Core terms of use.

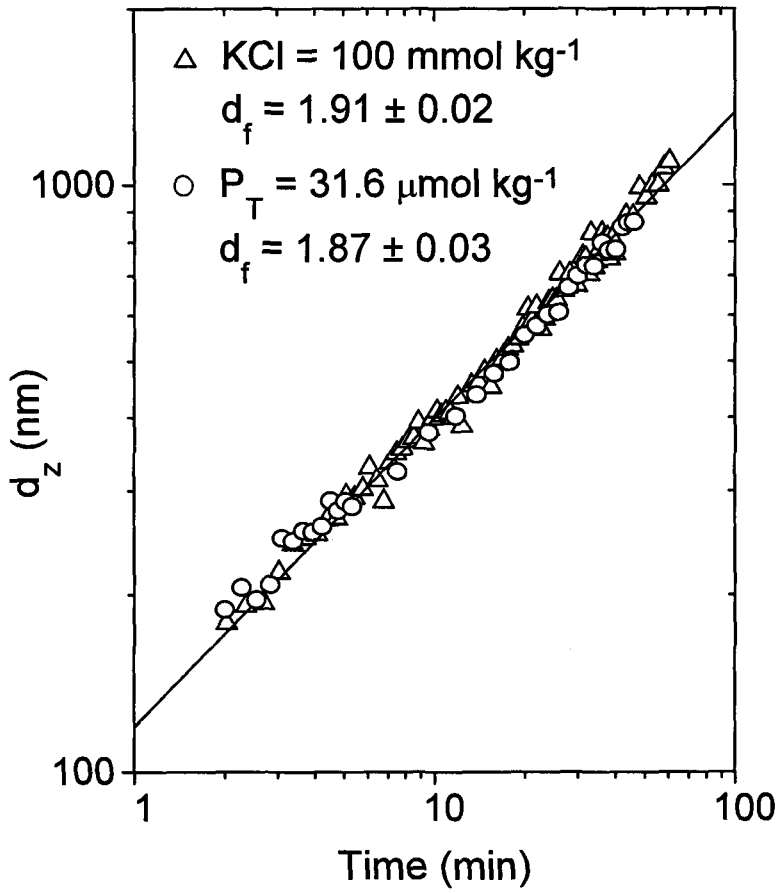


Figure 6. Log–log plot of d_z versus coagulation time for DLA: KCl = 100 mmol kg^{-1} (Δ), P_T = 31.6 μmol kg^{-1} and I = 1.0 mM (○). Slope and 95% confidence intervals are shown. Hematite concentration = 10 mg L^{-1}, pH = 6.0, T = 25 °C.

$$S_R = \frac{R_{DLA}}{R_{exp}} \quad [7]$$

Plots of log S_R versus KCl and P_T concentrations are shown in Figures 5c and 5d. The graphs in Figure 5 provide a concise and convenient summary of the coagulation kinetics. A rapid decrease in S_R is observed with increasing KCl to the CCC at 80 mmol kg^{-1} (Figure 5c), which results in the maximum observed d_z (30 min) (Figure 5a). For phosphate-induced coagulation at 1.0 mmol kg^{-1} total ionic strength, a sharp maximum in d_z (30 min) is observed at the p.z.c., log P_T = −4.5 (Figure 5b). Positive (P_T < p.z.c.) and negative (P_T > p.z.c.) charge development results in large decreases in the initial coagulation rate (Figure 5d). Our results are in close agreement with a prior study (Liang and Morgan 1990) that employed light transmission measurements to determine a maximum coagulation rate at P_T = 20 μM for 10 mg kg^{-1} hematite suspensions. Liang and Morgan (1990) found that their kinetic data were consistent with surface complexation modeling if phosphate adsorption was assumed to result in mononuclear, inner-sphere complexes with surface Fe via a ligand exchange mechanism.

Aggregate Structure

In DLA, log–log plots of d_z versus time are linear with a slope equal to the inverse of the fractal dimension, d_f (Equation [4]). Representative kinetic data for DLA are plotted on log scale in Figure 6. The dynamic scaling results for d_f of aggregates formed in the presence of excess KCl ([KCl] ≥ CCC) are identical to those reported by Zhang and Buffle (1996) for hematite at pH 3 where the CCC is 100 mM. Furthermore, d_f values for DLA are equivalent for systems where aggregation was induced by counterion screening or surface charge neutralization (Figure 6). That is, according to dynamic scaling of size evolution data, the value of d_f for aggregates formed at [KCl] ≥ CCC is equal to that obtained for aggregates formed at P_T = p.z.c.

Static light scattering experiments can provide a measure of d_f over a broader range of electrolyte concentrations encompassing both DLA and RLA regimes

Downloaded from https://www.cambridge.org/core. 16 Nov 2026 at 11:32:43, subject to the Cambridge Core terms of use.

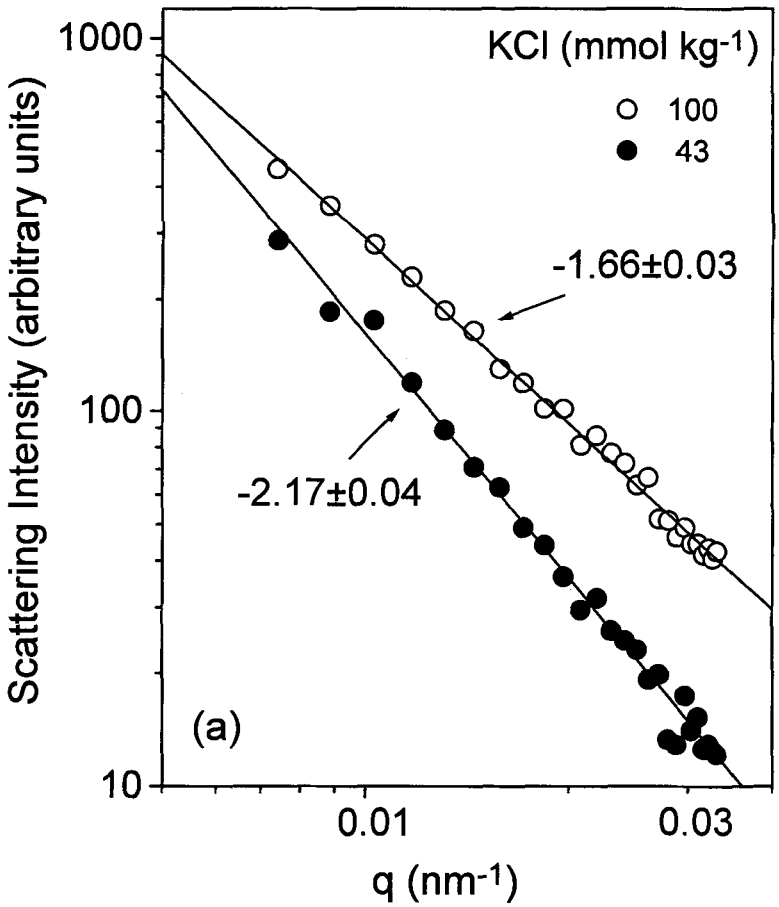


Figure 7. Representative static light scattering data for aggregates formed by (a) Cl^- screening and (b) phosphate adsorption (I = 1.0 mM). Slope and 95% confidence intervals are shown. Hematite concentration = 10 mg L^{-1}, pH = 6.0, T = 25 °C.

(Schmidt 1989; Zhang and Buffle 1996). The scattering intensity (arbitrary units) of aggregates with d_z greater than 1.0 μm was measured over the range of scattering angles 20–150°. Representative scattering intensity data are plotted versus wavevector (q) for Cl^- (Figure 7a) and $H_2PO_4^-$ (Figure 7b) induced aggregation. The slope of each curve gives the magnitude of the scattering exponent, n, which is shown for selected experiments on each graph. The value of n is equal to d_f if Equation [5] is valid. Static light scattering data for DLA where KCl = 100 mmol kg^{-1} and P_T = 31.6 μmol kg^{-1} can be compared with the dynamic scaling data presented in Figure 6. The values of n determined by SLS for DLA are roughly equivalent for the 2 treatments (Cl^- versus $H_2PO_4^-$ induced aggregation). However, the n values obtained for the DLA regime by SLS are lower (by approximately 0.2) than d_f values calculated by dynamic scaling of kinetic data (Equation [4]). Values of n less than d_f may be due to the fact that assumptions regarding the validity of Equation [5] are not strictly satisfied. For a given d_f, the cut-off distance, ξ, may be estimated from Equation [6] and the fact that the true hydrodynamic diameter may be up to 2-fold larger than d_z because of the rotational motion of the aggregates (Weitz et al. 1985). Our SLS measurements were performed at scattering angles of 20 to 150°, which, for d_f = 1.8 and $R_g \approx \xi$ = 1000 nm, correspond to qr_o of 0.155 to 0.863 and $q\xi$ of 6 to 33, respectively. Therefore, the conditions $qr_o \ll 1$ and $q\xi \gg 1$ are not strictly satisfied over the entire q range.

To investigate the effects of finite aggregate and primary particle size, we have calculated the theoretical scattering intensity for different ξ values according to Mie theory using the approach detailed in Zhang and Buffle (1996). The real and imaginary refractive indices of hematite were set equal to 2.34 and 0.17, respectively (Kerker et al. 1979). For r_o = 25 nm and d_f = 1.8, the value of n decreases with decreasing aggregate size. The calculated values of n for our experimental conditions are 1.72 (ξ = ∞), 1.70 (ξ = 1000 nm), 1.65 (ξ = 500 nm) and 1.53 (ξ = 250 nm). The scattering exponent underestimates d_f even for aggregates of infinite size because the condition $qr_o \ll 1$ is

Downloaded from https://www.cambridge.org/core. 16 Nov 2026 at 11:32:43, subject to the Cambridge Core terms of use.

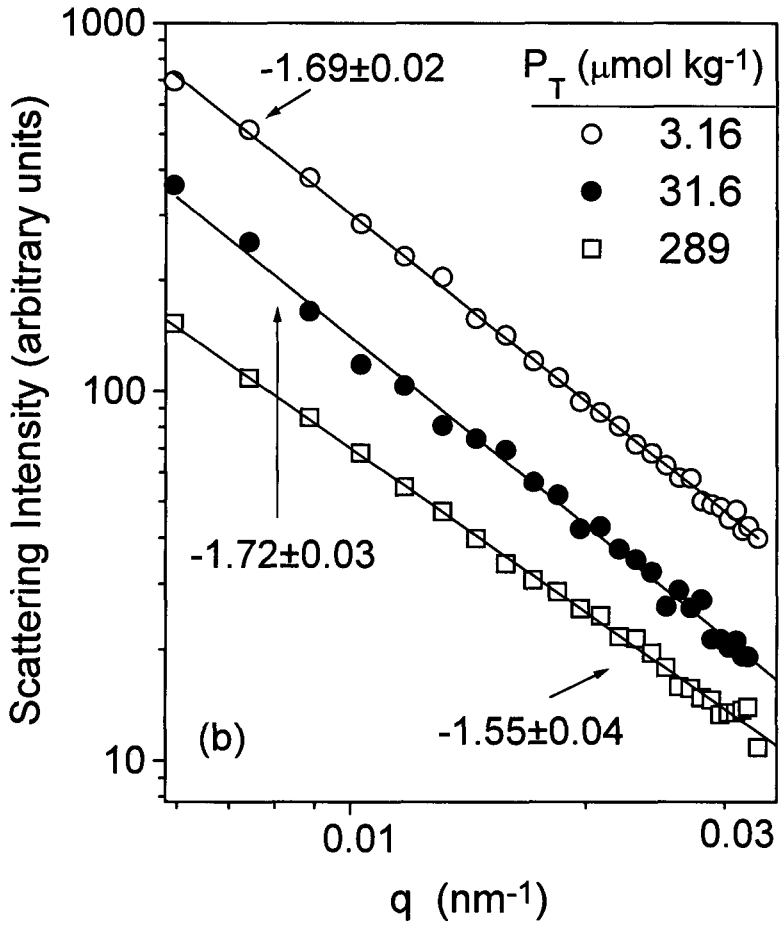


Figure 7. Continued

not satisfied. Since our SLS experiments were performed after the measured hydrodynamic diameter reached 1.0 μm, it is possible that the scattering exponent may underestimate d_f by as much as 0.2. This calculated difference is consistent with that which separates our dynamic scaling (1.9) and SLS (1.7) estimates of aggregate fractal dimensions. The former estimates represent the upper limit of d_f, whereas n may be considered to represent the lower limit (Zhang and Buffle 1995, 1996).

Figure 7 shows that, under RLA conditions, electrolyte composition exerts a large influence on measured values of n depending on whether the effect of electrolyte is due to charge screening (Cl^-) or charge neutralization by surface complexation ($H_2PO_4^-$). As KCl concentration is decreased below the CCC to 43 mmol kg^{-1}, n increases from 1.7 to 2.2 (Figure 7a), corresponding to more compact aggregates consistent with cluster–cluster aggregation theory (Jullien and Botet 1987). However, no increase in n is observed with decreasing or increasing phosphate concentration to below or above the p.z.c. (31.6 μmol kg^{-1}). These results are exemplified by plotting n, as measured by SLS, versus log S_R for all experiments where both parameters were measured (Figure 8). For KCl-induced aggregation, an increase in particle packing density [increase in n] is observed as initial coagulation rate is decreased (S_R is increased) over 1 order of magnitude (Figure 8a). Conversely, for phosphate-induced aggregation there is no clear trend in n as a function of S_R (Figure 8b) or P_T (Figure 9), even though S_R spans nearly 3 orders of magnitude (Figure 8b). According to Figure 8b and Figure 9, aggregates formed at $P_T >$ p.z.c. exhibit consistently lower apparent fractal dimensions (n) than those formed at the p.z.c. Below the p.z.c., results are more variable. However, aggregates formed as a result of surface charge neutralization (that is, by surface complexation of phosphate), at P_T greater than or less than the p.z.c., yield lower values of n than aggregates formed as a result of counterion screening (that is, in the presence of excess KCl).

The TEM observations are consistent with light scattering data. In KCl solution, loose structures result from conditions of DLA (Figure 10a, KCl = 90 mmol

Downloaded from https://www.cambridge.org/core. 16 Nov 2026 at 11:32:43, subject to the Cambridge Core terms of use.

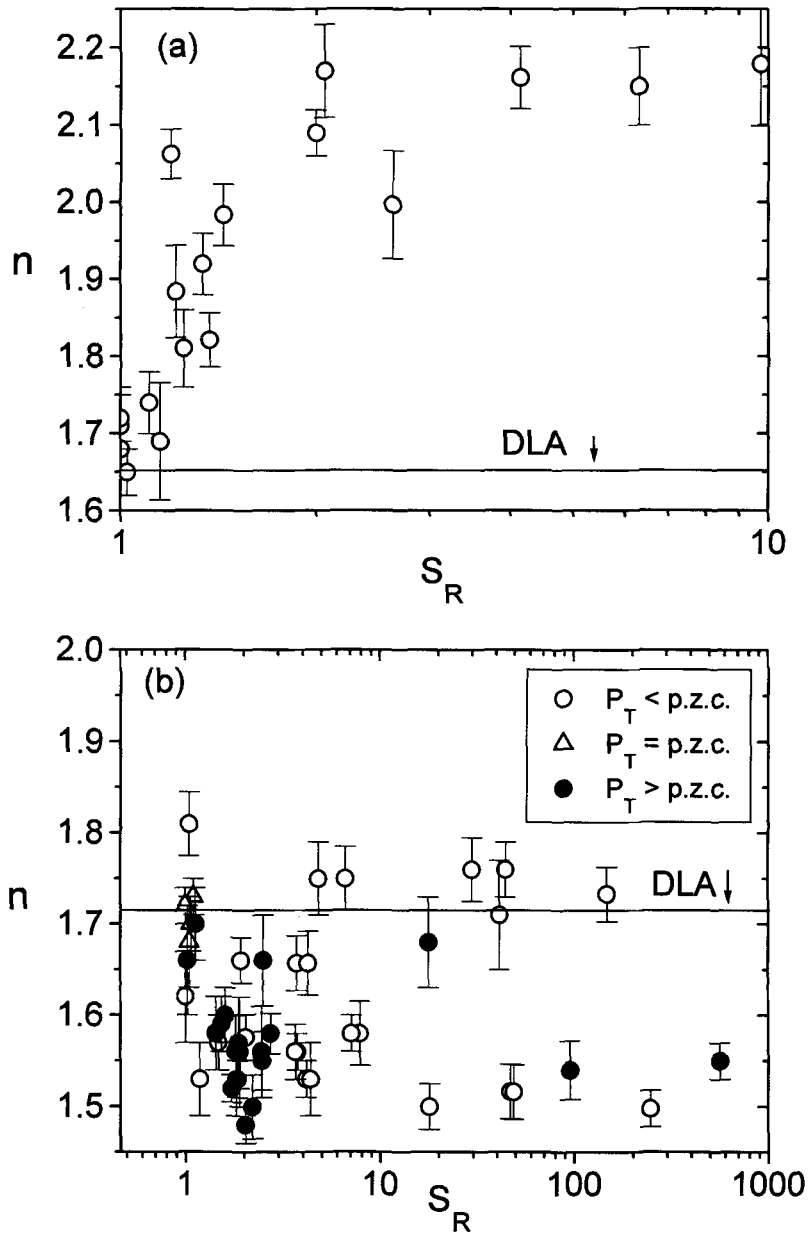


Figure 8. Apparent fractal dimension (n) of aggregates as measured by SLS versus relative stability: (a) KCl-induced aggregation; (b) phosphate-induced aggregation (I = 1.0 mM). Hematite concentration = 10 mg L^{-1}, pH = 6.0, T = 25 °C. Error bars indicate 95% confidence intervals. Measured values of n corresponding to DLA are shown for reference.

kg^{-1}), whereas more compact aggregates are formed when [KCl] < CCC (Figure 10b, KCl = 39 mmol kg^{-1}). Aggregation of hematite in the presence of phosphate at P_T = p.z.c. results in loose structures (Figure 11b, P_T = 31.6 μmol kg^{-1}) that are comparable to those observed following coagulation in systems with [KCl] ≥ CCC (Figure 10a). However, in contrast to KCl-induced aggregation, very loose structures are also observed under conditions of phosphate-induced slow coagulation both below (Figure 11a, P_T = 3.2 μmol kg^{-1}) and above (Figure 11c, P_T = 262 μmol kg^{-1}) the p.z.c.

DISCUSSION

In the absence of specifically adsorbing ions other than H^+ and OH^-, the hematite surface is net-positive-charged at pH 6.0 (Figure 2). At a given KCl concentration, the coagulation rate at pH 6 is higher than at pH 3 (Zhang and Buffle 1995) because of the increase in net adsorbed proton charge with de-

Downloaded from https://www.cambridge.org/core. 16 Nov 2026 at 11:32:43, subject to the Cambridge Core terms of use.

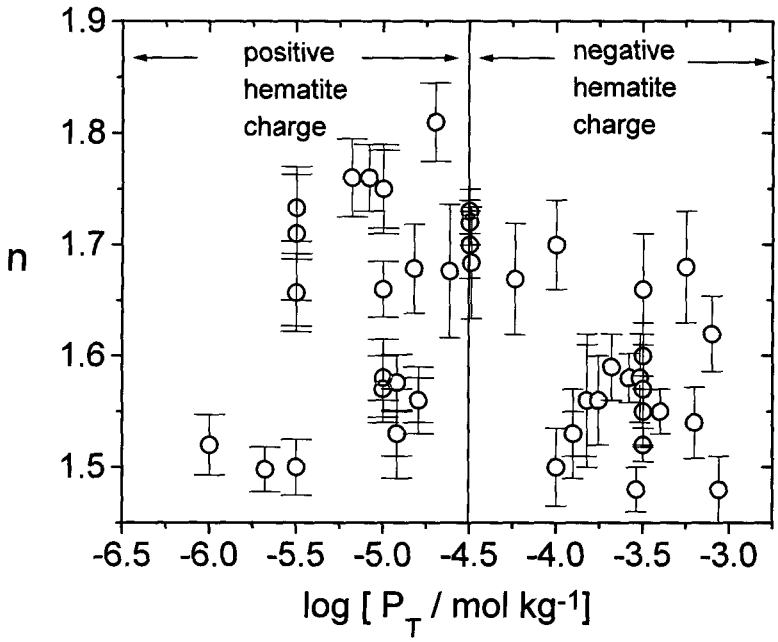


Figure 9. Apparent fractal dimension (n) of aggregates formed in the presence of phosphate versus phosphate concentration (I = 1.0 mM). Hematite concentration = 10 mg L^{-1}, pH = 6.0, T = 25 °C. Error bars indicate 95% confidence intervals.

creasing pH (Penners et al. 1986; Colic et al. 1991). Thus, the CCC for hematite in KCl solution at pH 6 (80 mM) is significantly lower than that at pH 3 (100 mM). Both counterion screening and surface-charge neutralization are capable of producing a range of kinetic coagulation phenomena, depending upon the concentration of counterion and complexing adsorbate, respectively (Figures 3–5). In contrast to our study, Carpineti et al. (1990) measured lower aggregate d_f values for DLA induced by counterion screening than those reported for aggregates formed by surface charge neutralization with H^+ (Lin et al. 1989). In the present work, no differences in structure for aggregates formed by charge screening or charge neutralization in the DLA regime were detectable by dynamic scaling of kinetic data (Figure 6), SLS (Figure 7) or TEM observations (Figures 10a and 11b). The values of d_f obtained for DLA are within the range reported in previous studies of colloidal hematite (Zhang and Buffle 1996), goethite (Hackley and Anderson 1989), gold, silica and latex (Lin et al. 1989; Carpineti et al. 1990).

The d_f values obtained from our SLS and dynamic scaling experiments represent the lower and upper limits, respectively, of the hematite aggregate fractal dimensions. Dynamic scaling of coagulation data requires that the ratio of d_z to R_g is constant so that Equation [4] may be applied to time-dependent measurements of d_z. Calculations indicate that this ratio is constant for our experimental conditions at $d_z > 200$ nm (Zhang and Buffle 1995), although small increases with aggregate size have been suggested by others (Lin et al. 1989). An increase in the ratio with aggregate size for $d_z > 200$ nm would lead to decreased slopes in Figure 6, and overestimation of d_f. Therefore, the inverse of the slopes in Figure 6 represent the upper limit of the fractal dimension for aggregates formed in the DLA regime. Conversely, the specific conditions for equality of the SLS scattering exponent (Figures 7–8) and d_f are not rigorously satisfied. The finite size of primary particles and aggregates may produce an underestimate of d_f in this case. However, model calculations indicate that the scattering exponent underestimates d_f by a maximum of 0.2.

Numerous previous studies have shown an inverse relation between d_f and coagulation rate (Lin et al. 1989; Hackley and Anderson 1989; Amal et al. 1990; Asnaghi et al. 1992; Zhang and Buffle 1996) and this pattern is observed in the present study for aggregates formed by counterion screening in the presence of KCl (Figure 8a). However, the coagulation rate for phosphate-induced destabilization (Figure 8b) shows a completely different trend. Aggregates thus formed show more open structure comprising linear chains of hematite particles (Figure 11) with scattering exponent or d_f values even smaller than those obtained in DLA conditions (Figure 8b, Figure 9).

These results may be interpreted in terms of previous work regarding complexation of phosphate on iron oxide surfaces. Infrared spectroscopic analyses

Downloaded from https://www.cambridge.org/core. 16 Nov 2026 at 11:32:43, subject to the Cambridge Core terms of use.

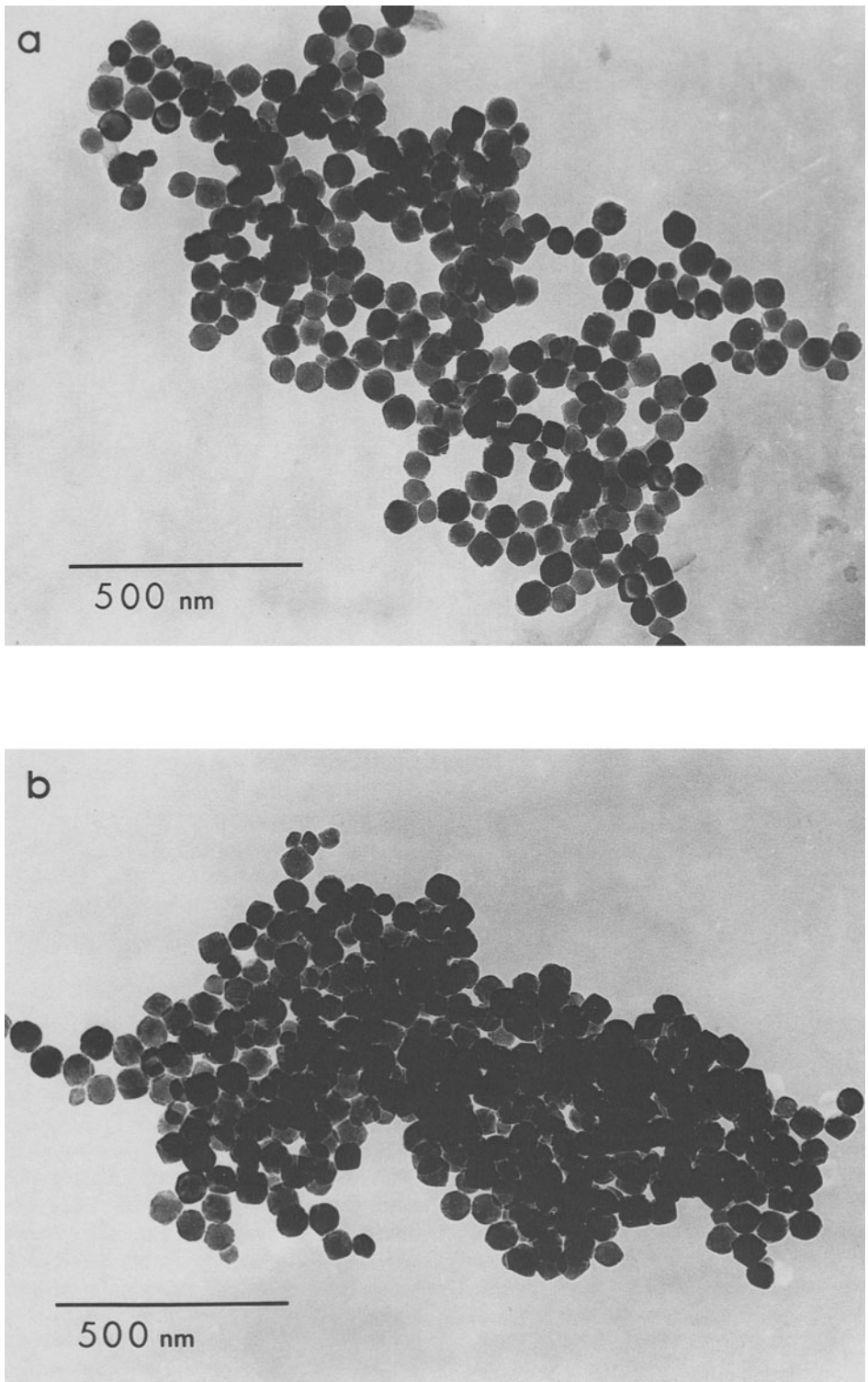


Figure 10. TEM micrographs of aggregates formed by counterion screening of surface charge. KCl concentrations are (a) 90 and (b) 39 mmol kg^{-1}. Hematite concentration = 10 mg L^{-1}, pH = 6.0, T = 25 °C.

Downloaded from https://www.cambridge.org/core. 16 Nov 2026 at 11:32:43, subject to the Cambridge Core terms of use.

of phosphate–goethite interactions indicate that high-affinity, binuclear surface complexes form by ligand exchange at sites comprising 2 contiguous singly coordinated ("type *A*") surface hydroxyl groups (Russell et al. 1974; Parfitt and Atkinson 1976; Parfitt et al. 1976; Tejedor–Tejedor and Anderson 1990). Therefore, phosphate is preferentially adsorbed on *crystal faces* comprising contiguous *A* hydroxyls. Synthetic goethites appear as needles or lathes in the *c* direction and approximately 90% of the total surface contains crystal faces with contiguous hydroxyl functional groups. However, only a fraction of the nonbasal faces of the hematite surface would be suitable for the formation of binuclear surface complexes (Colombo et al. 1994; Barrón and Torrent 1996). If phosphate forms inner-sphere complexes at specific sites that are distributed nonrandomly over the hematite surface in accordance with crystallographic faces, then particle sticking may be anisotropic because it is limited by the coalescence of positive and negative charged faces. The aggregates thus formed would be less compact because of crystallographic constraints on aggregate structure. In contrast, in the case of counterion screening, several ineffective encounters may occur as a particle migrates to the interior of an aggregate where it will stick, producing a more compact structure (Evans and Wennerström 1994).

Few observations of anisotropic aggregation of metal oxide particles have been reported. Hackley and Anderson (1989) suggested that crystallographic preferences caused nonrandom (anisotropic) sticking of goethite (α-FeOOH) particles in NaCl during DLA. They measured a value of d_f equal to 1.6 for DLA and attributed this low value to preferential sticking of the predominant (100) faces of goethite; these faces would provide a maximum surface area for attractive van der Waals interaction in DLA when electrostatic repulsive forces are diminished.

The oscillations observed in size versus time data at high P_T (Figure 4b) are suggestive of fragmentation and coagulation (reorganization) processes. This behavior was consistently observed and may be related to phosphorus adsorption–desorption dynamics, although further work is required to establish a direct relationship. The formation of mononuclear inner-sphere complexes between phosphate and solid-phase Fe(III) may enhance hematite dissolution by polarizing Fe-O bonds on the oxide surface (Stumm and Furrer 1987), which could cause fragmentation of aggregates, but no measureable increase in dissolved Fe was observed with either increasing P_T or increasing reaction time. Dissolution of Fe may actually be inhibited if phosphate forms binuclear complexes with the hematite surface (Stumm and Furrer 1987). At $P_T >$ p.z.c., surface *P* concentration is high enough to induce charge reversal and, therefore, adsorption is probably not limited to that portion of the surface comprising contiguous *A* type hydroxyls. However, loose and open floccules are formed under conditions of slow coagulation at $P_T >$ p.z.c. (Figures 7b, 8b, 11c), which suggests that a nonrandom distribution of surface charge is persistent to high adsorbed phosphate concentrations.

One possible cause for the oscillations in d_z at high P_T is that weakly adsorbed phosphate, which contributes to the high (negative) surface charge, favors fragmentation and aggregate reorganization. Subsequent particle collisions may result in expulsion of this weakly sorbed phosphate, concurrent with the formation of open-structured aggregates. This hypothesis is consistent with previous research. Anderson et al. (1985) found that initial phosphate uptake increased, and oscillation in uptake was more apparent, with decreasing goethite:phosphate ratio. These authors suggested that contact between adjacent particles caused expulsion of some phosphate (hence desorption was observed). In addition, the greater order of phosphate-treated aggregates observed in electron and X-ray diffraction patterns was attributed to phosphate bridging of goethite particles (Anderson et al. 1985).

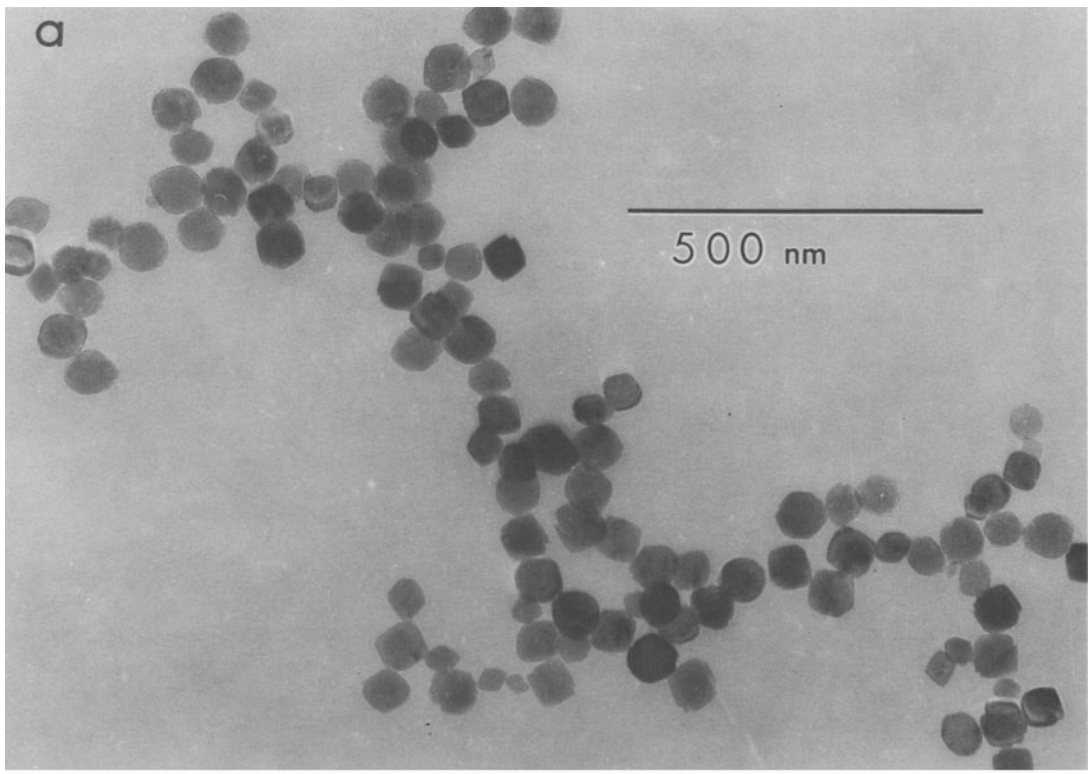
CONCLUSIONS

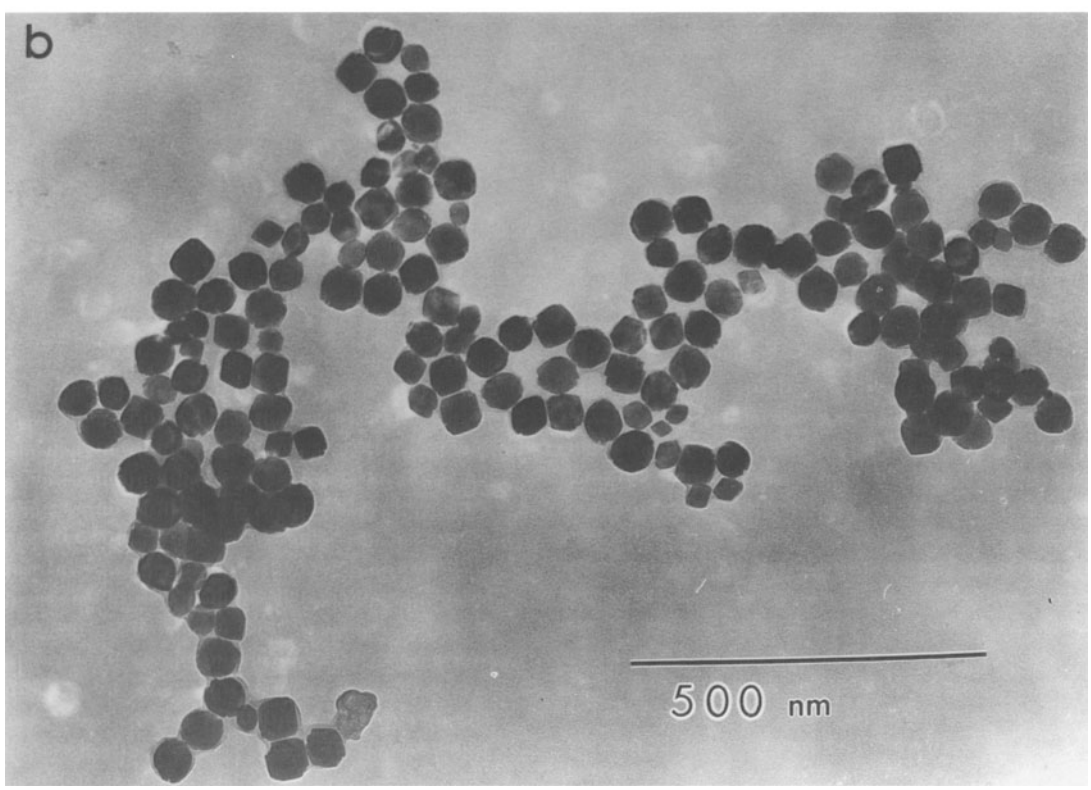
Colloidal hematite suspensions may be destabilized by increasing indifferent electrolyte concentration or by reducing the magnitude of particle surface charge. When phosphate is used to affect surface charge, the structure of resulting aggregates differs markedly from the structure of aggregates formed in the presence of KCl, except for the DLA case. Diffusion-limited aggregation produces aggregates of d_f = 1.7–1.9 with lower values measured by SLS and higher values determined from dynamic scaling of kinetic data. Aggregates formed in KCl show an increase in d_f from 1.7 to 2.2, measured by SLS, with a 10-fold increase in the relative stability. In contrast, phosphate-induced aggregation always leads to the formation of loose, open structures of low d_f (<1.8 by SLS) and no relationship between coagulation kinetics and d_f is observed over a several hundred-fold increase in the stability ratio. The results of this study indicate that the manner in which a colloidal hematite suspension is destabilized may significantly affect the structure of resulting aggregates and this structure may not be accurately predicted from kinetic data on the time evolution of aggregate size.

ACKNOWLEDGMENTS

The authors are grateful to R. Ferretti for measurements of primary particle size of the hematite by TEM and to the manuscript reviewers for helpful comments. The research reported in this paper was supported in part by National Sciences Foundation grant INT-9302228 and by Swiss National Foundation grant 2000-037598·93/1.

Downloaded from https://www.cambridge.org/core. 16 Nov 2026 at 11:32:43, subject to the Cambridge Core terms of use.





Downloaded from https://www.cambridge.org/core. 16 Nov 2026 at 11:32:43, subject to the Cambridge Core terms of use.

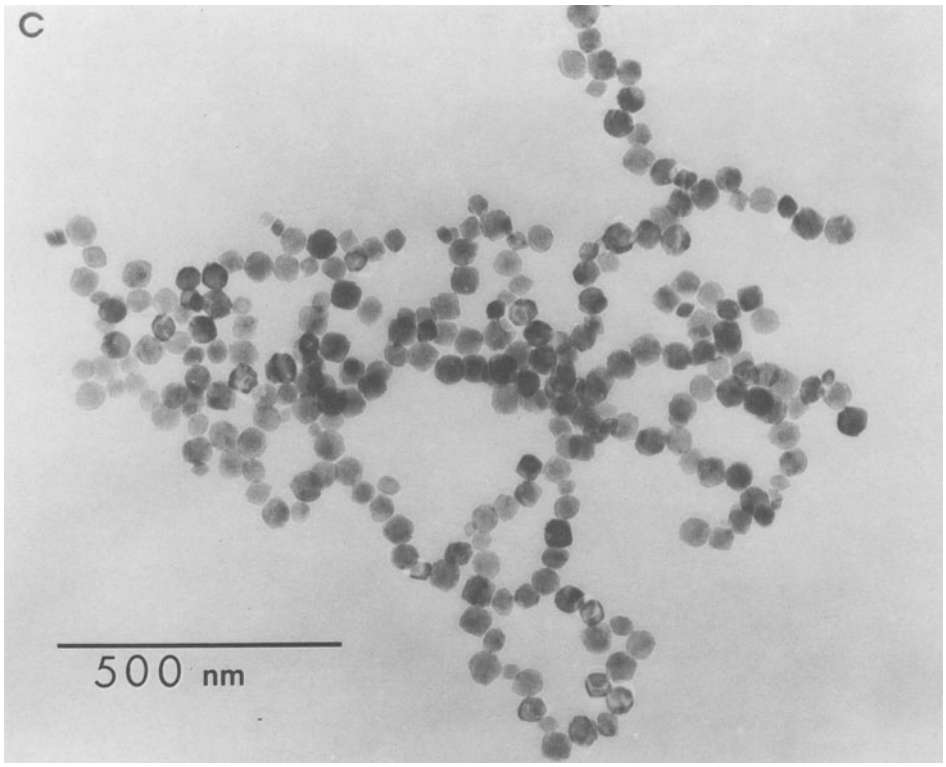


Figure 11. Continued

REFERENCES

Amal R, Raper JA, Waite TD. 1990. Fractal structure of hematite aggregates. J Colloid Interface Sci 140:158–168.

Anderson MA, Tejedor–Tejedor MI, Stanforth RR. 1985. Influence of aggregation on the uptake kinetics of phosphate by goethite. Environ Sci Technol 19:632–637.

Asnaghi D, Carpineti M, Giglio M, Sozzi M. 1992. Coagulation kinetics and aggregate morphology in the intermediate regimes between diffusion-limited and reaction-limited cluster aggregation. Phys Rev A 45:1018–1023.

Barrón V, Torrent J. 1996. Surface hydroxyl configuration of various crystal faces of hematite and goethite. J Colloid Interface Sci 177:407–410.

Carpineti M, Ferri F, Giglio M, Paganini E, Perini U. 1990. Salt-induced fast aggregation of polystyrene latex. Phys Rev A 42:7347–7354.

Colic M, Fuerstenau DW, Kallay N, Matijevic E. 1991. Lyotropic effect in surface charge, electrokinetics, and coagulation of a hematite dispersion. Colloid Surf 59:169–185.

Columbo C, Barrón V, Torrent J. 1994. Phosphate adsorption and desorption in relation to morphology and crystal properties of synthetic hematites. Geochim Cosmochim Acta 58:1261–1269.

Evans DF, Wennerström H. 1994. The colloidal domain. New York: VCH. 515 p.

Frosh D, Westphal C. 1989. Melamime resins and their application in electron microscopy. Electron Microsc Rev 2: 231–255.

Hackley VA, Anderson MA. 1989. Effects of short-range forces on the long range structure of hydrous iron-oxide aggregates. Langmuir 5:191–198.

Hunter RJ. 1987. Foundations of colloid science, vol. 1. New York: Oxford Univ Pr. 673 p.

Jullien R, Botet R. 1987. Aggregation and fractal aggregates. Singapore: World Scientific. 120 p.

Kerker M, Sheiner P, Cooke DD, Kratohvil JP. 1979. Adsorption index and color of colloidal hematite. J Colloid Interface Sci 71:176–187.

Liang L, Morgan JJ. 1990. Chemical aspects of iron oxide coagulation in water: Laboratory studies and implications for natural systems. Aquatic Sci 52:32–55.

Lin MY, Lindsay HM, Weitz DA, Ball RC, Klein R, Meakin P. 1989. Universality of fractal aggregates as probed by light scattering. Proc R Soc Lond A 423:71–87.

Meakin P. 1991. Fractal aggregates in geophysics. Rev Geophys 29:317–331.

Murphy J, Riley JP. 1962. A modified single solution method for the determination of phosphate in natural waters. Anal Chim Acta 27:31–36.

O'Melia CR. 1989. Particle–particle interactions in aquatic systems. Colloid Surf 39:255–271.

←

Figure 11. TEM micrographs of aggregates formed by neutralization of surface charge at increasing total phosphate concentration: P_T = (a) 3.2 μmol kg^{-1} (<p.z.c.), (b) 31.2 μmol kg^{-1} (= p.z.c.) and (c) P_T = 262 μmol kg^{-1} (>p.z.c.). Hematite concentration = 10 mg L^{-1}, pH = 6.0, I = 1.0 mM, T = 25 °C.

Downloaded from https://www.cambridge.org/core. 16 Nov 2026 at 11:32:43, subject to the Cambridge Core terms of use.

Parfitt RL, Atkinson RJ. 1976. Phosphate adsorption on goethite (α-FeOOH). Nature 264:740–742.

Parfitt RL, Russell JD, Farmer VC. 1976. Confirmation of the surface structures of goethite (α-FeOOH) and phosphated goethite by infrared spectroscopy. J Chem Soc Faraday Trans 1 72:1082–1087.

Pecora R. 1985. Dynamic light scattering. New York: Plenum Publishing. 420 p.

Penners NHG, Koopal LK. 1986. Preparation and optical properties of homodisperse haematite hydrosols. Colloid Surf 19:337–349.

Penners NHG, Koopal LK, Lyklema J. 1986. Interfacial electrochemistry of haematite (α-Fe_2O_3): Homodisperse and heterodisperse sols. Colloid Surf 21:457–468.

Perret D, Leppard GG, Müller MM, Belzile N, De Vitre R, Buffle J. 1992. Electron microscopy of aquatic colloids: Non-perturbing preparation of specimens in the field. Wat Res 25:333–1343.

Pfeifer P, Obert M. 1989. Fractals: Basic concepts and terminology. In: Avnir D, editor. The fractal approach to heterogeneous chemistry. New York: J. Wiley. p. 11–43.

Russell JD, Parfitt RL, Fraser AR, Farmer VC. 1974. Surface structures of gibbsite, goethite, and phosphated goethite. Nature 248:220–221.

Schmidt PW. 1989. Use of scattering to determine the fractal dimension. In: Avnir D, editor. The fractal approach to heterogeneous chemistry. New York: J. Wiley. p 67–79.

Schurtenberger P, Newman M. 1993. Characterization of biological and environmental particles using static and dynamic light scattering. In: Buffle J, van Leeuwen H, editors. Environmental particles, vol. 2. Boca Raton, FL: Lewis Publishers. p 37–115.

Sigg L, Stumm W. 1981. The interaction of anions and weak acids with the hydrous goethite surface. Colloid Surf 2: 101–117.

Sposito G. 1992. Characterization of particle surface charge. In: Buffle J, van Leeuwen H, editors. Environmental particles, vol. 1. Boca Raton, FL: Lewis Publishers. p 291–314.

Sposito G. 1994. Chemical equilibria and kinetics in soils. New York: Oxford Univ Pr. 268 p.

Stumm W, Furrer G. 1987. The dissolution of oxides and aluminum silicates: Examples of surface-coordination controlled kinetics. In: Stumm W, editor. Aquatic surface chemistry. New York: J. Wiley. p 197–219.

Stumm W, Morgan JJ. 1996. Aquatic chemistry, 3rd ed. New York: J. Wiley. 1022 p.

Teixeira J. 1986. Experimental methods for studying fractal aggregates. In: Stanley HE, Ostrowski N, editors. On growth and form: Fractal and non-fractal patterns in physics. Dordrecht: Martinus-Nijhoff. p 145–162.

Teixeira J. 1988. Small-angle scattering by fractal systems. J Appl Cryst 21:781–785.

Tejedor–Tejedor MI, Anderson M. 1990. Protonation of phosphate on the surface of goethite as studied by CIR-FTIR and electrophoretic mobility. Langmuir 6:602–611.

Verwey EJW, Overbeek JTG. 1948. Theory of the stability of lyophobic colloids. Amsterdam: Elsevier. 205 p.

Weitz DA, Huang JS, Lin MY, Sung J. 1985. Limits of the fractal dimension for irreversible kinetic aggregation of gold colloids. Phys Rev Lett 54:1416–1421.

Zhang J, Buffle J. 1995. Kinetics of hematite aggregation by polyacrylic acid. J Colloid Interface Sci 174:500–509.

Zhang J, Buffle J. 1996. Multi-method determination of the fractal dimension of hematite aggregates. Colloid Surf A 107:175–188.

(Received 5 June 1996; accepted 6 December 1996; Ms. 2775)

Downloaded from https://www.cambridge.org/core. 16 Nov 2026 at 11:32:43, subject to the Cambridge Core terms of use.